DOI: 10.1002/chem.200902118

Evaporation-Induced Ordered Honeycomb Structures of Gold Nanoparticles at the Air/Water Interface

Hongmin Ma and Jingcheng Hao*[a]

Abstract: The breath figure method was used to prepare dodecanethiol-capped gold nanoparticle macroporous structures with pore diameters from 1.7 to 3.5 μm on an air/water interface. A two-step procedure is proposed for the fabrication of these macroporous structures, by forming a surfactant monolayer on water, and drop-casting a gold nanoparticle dispersion in chloroform onto the surfactant monolayer. The self-assembled films are easily transferred from the water surface onto different substrates and were characterized by TEM, SEM, and AFM. Ordered honeycomb structures with different pore arrays (perforated monolayer films, hexagonal networks and alveoli-like porous films) were obtained. The change in morphology is concentration dependent, and deformed structures with elliptic honeycomb networks are also observed. In addition, honeycomb films using gold nanoparticles stabilized by a weakly bound ligand (dioctadecyldimethylammonium chloride) were formed by the same technique. These films have potential as substrates for surface-enhanced Raman spectroscopy.

Keywords: gold · honeycomb structures · nanoparticles · self-assembly · surfactants

Introduction

Self-assembly of nanoparticles into ordered structures has become an important approach to construct novel mesoscale materials because of the unique size-dependent optical, electronic and magnetic properties of nanoparticles.[1] In the past decade, many experiments have focused on the self-assembly of ligand-stabilized nanoparticles into two- or three-dimensional superlattices.[2] In practice however, some applications such as sensors,[3] photonic crystals,[4] and spectroscopic analysis[5] require complex macroporous ordered structures to be effective. Colloidal crystals,[6] emulsions,[7] and even bacteria[8] may be used as templates to form ordered macroporous materials. In most cases a templated fabrication involves multiple steps, such as removal of the template, which increases the complexity of the fabrication process and may result in damage to the final structures. Thus, the development of single-step, template-free processes for macroporous-structure fabrication are of considerable interest.

One important macroporous structure is a honeycomb-patterned thin film with hexagonally ordered arrays of macropores. Fabrication of honeycomb films using condensed water droplets as a dynamic template, the so-called "breath figure" method, is well established for a variety of polymers. Macroporous polymer films may generally be formed on solid surfaces[9,10] but also may form on a fluid surface.[11] Shimomura and co-workers have reported the fabrication of honeycomb films of an amphiphilic copolymer at the air/water interface.[12] Formation of nanoparticle-based ordered honeycomb structures based on water droplet condensation was also reported.[4,13–15] Recent studies showed that the production of breath figures is a fairly general method to construct hierarchical architectures of nanoparticles.[3,16] However, specially controlled conditions, such as high relative humidity or moist airflow, are necessary for these preparation methods. In addition, honeycomb films formed on solid substrates cannot be easily transferred to other substrates for different applications because nanoparticle-based films are more fragile than polymer films.

Recently, we reported the formation of highly ordered honeycomb films made of polyoxometalate-based, surfactant-encapsulated clusters at an air/water interface.[17] The self-assembled thin films were easily transferred from the surface of the water to a variety of solid substrates. This

[a] H. Ma, Prof. Dr. J. Hao
Key Laboratory of Colloid and Interface Chemistry
Shandong University, Ministry of Education, Jinan 250100 (China)
Fax: (+86) 531-8856-4750
E-mail: jhao@sdu.edu.cn

Supporting information for this article is available on the WWW under http://dx.doi.org/10.1002/chem.200902118.

technique will promote the use of such mesoscale ordered structures in different areas of application. In this work, we propose a simple, low-cost, two-step process for the fabrication of gold nanoparticle-based macroporous structures based on solvent evaporation. To the best of our knowledge, this is the first report on the formation of ordered honeycomb structures of ligand-stabilized gold nanoparticles at an air/water interface. These metallic thin films with porous morphologies may be useful as substrates for applications in catalysis and surface-enhanced Raman spectroscopy.

Results and Discussion

The strategy for formation of thin films with ordered honeycomb structures is illustrated in Figure 1. A surfactant monolayer is formed on water surface by spreading a chloroform solution of dioctadecyldimethylammonium chloride (DODMAC) to ensure that the gold nanoparticle dispersions for film fabrication can form a stable liquid film on water surface. After a gold nanoparticle dispersion is dropped on the water surface, the rapid evaporation of the solvent decreases the air/liquid interfacial temperature below its dew point, resulting in the condensation of microscopic water droplets on the surface of solution. The water droplets self-assemble into ordered arrays under the effects of thermocapillary forces and Marangoni convection.[18] Continued evaporation casts the gold nanoparticles into structures around the organized water droplets. When the solvent and water droplets evaporate completely, an ordered film with the imprint of the water droplets is formed. As the pore formation relies on water droplet condensation during solvent evaporation, previous researchers have supplied the droplets using specially-controlled high relative humidity chambers or by passing a moist airflow across samples fabricated on solid substrates. In our strategy, the high relative humidity at the air/water interface provides the necessary water vapor for the condensation of water droplets to template the formation of the porous structures.

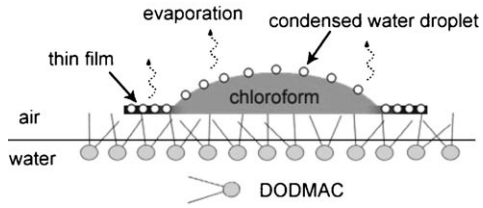

Figure 1. Illustration of the breath figure film formation at an air/water interface.

Dodecanethiol-capped gold nanoparticles with an average core diameter of 4.5 nm (Figure 2a) were used for the fabrication of honeycomb structures. In contrast to previous reports describing a single thin film structure formed on solid substrates, three domains with distinct boundaries between them and different morphologies were observed from the margin to the center of the films cast on an air/water interface. Figure 2b–d show representative SEM images of the three different structures; we define these as a perforated monolayer film (Figure 2b), a hexagonal network (Figure 2c), and an alveoli-like porous film (Figure 2d), respectively. The morphological features of each structure are described below.

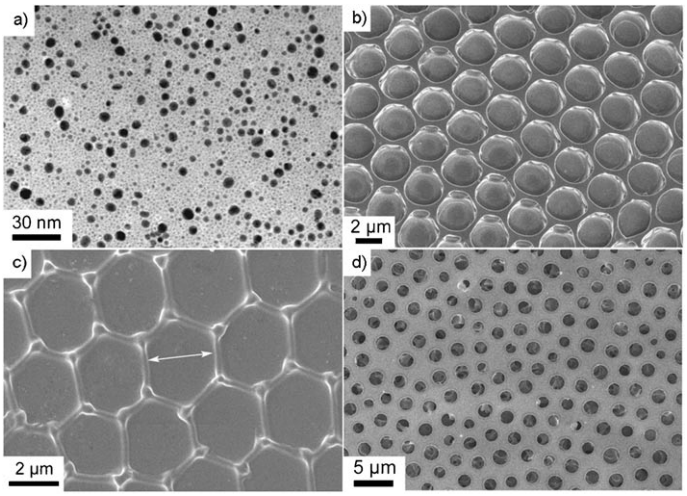

Figure 2. a) HRTEM image of the dodecanethiol-capped gold nanoparticles. SEM images of the three domains in the fabricated honeycomb films: b) a perforated monolayer film, c) a hexagonal network, and d) an alveoli-like porous film. The concentrations of gold nanoparticle dispersion for film fabrication: 0.6 $g L^{-1}$ (b and c), 0.8 $g L^{-1}$ (d).

The first morphology is exhibited as two-dimensional hexagonally ordered pore arrays which formed at the margin of the film. A through-pore structure (with two open-ended pores) can be observed from the TEM image of this perforated monolayer film domain (Figure 3a). From the enlarged SEM image one can also observed that adjacent pores are interconnected (Figure 3b). The two layers (top and bottom) of the film can be easily discerned and are con-

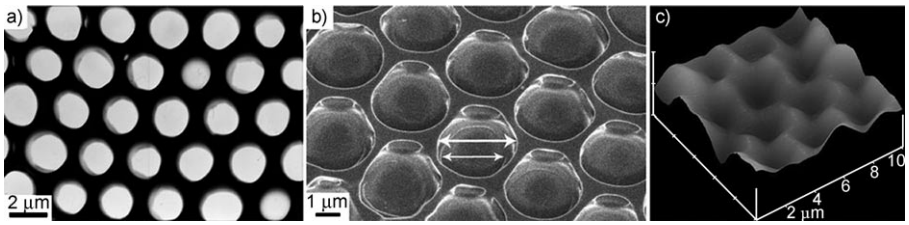

Figure 3. a) TEM, b) SEM and c) AFM images of the perforated monolayer domain. The arrows in b) indicate the pore diameter of the bottom (shorter) and top (longer) openings. The concentration of gold nanoparticle dispersion for film fabrication is 0.6 $g L^{-1}$.

nected at the interstitial positions of adjacent pores. A shift of the top layer with respect to the bottom layer can also be observed from the TEM image. The diameter of the openings at the bottom layer (average pore diameter 1.85 μm) is smaller than that of the upper openings which have an average diameter of 2.5 μm (as the arrows indicate in Figure 3b). Also because of the overlap of the two layers, the wall thickness obtained from the TEM image (0.8 μm) is larger than that obtained from the SEM image (0.35 μm). The average thickness of these perforated monolayer films obtained from the AFM image (Figure 3c) is 430 nm.

The second type of domain observed in the film is a hexagonal network with large nodes in the interconnected skeleton. These domains were present in the middle region of the fabricated film. The average pore diameter in these domains is larger (3.5 μm) than that of the perforated monolayer films (indicated by an arrow in Figure 2c); the wall thickness in this domain is also smaller (0.3 μm). The average height of the skeleton nodes obtained from AFM measurements (as the markers indicate in the top view image of Figure 4a) is 550 nm and is larger than that of the connected

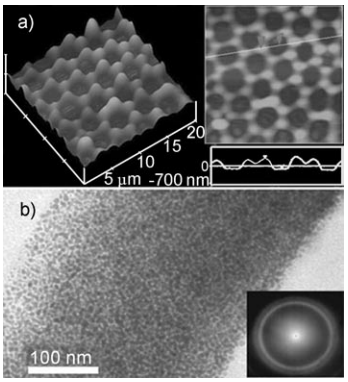

Figure 4. a) AFM and b) HRTEM images of the hexagonal networks. The inset in b) is the electron diffraction pattern of the network skeleton. The concentration of gold nanoparticle dispersion for film fabrication is 0.6 $g L^{-1}$.

parts which correspond to the sides of the hexagons. HRTEM studies confirm that the network skeletons are composed of tightly packed gold nanoparticles (Figure 4b) and the electron diffraction patterns (Figure 4b, inset) confirm the polycrystalline structures of the film.

The third type of domain is an alveoli-like porous structure formed in the central area of the fabricated thin film. The alveolar pores can be seen clearly in the enlarged SEM image (Figure 5a). The pore array on the surface of these domains is less ordered and the average diameter of the pore is smaller (1.7 μm). The AFM image (Figure 5b) illustrates that the pores on the surface are almost filled and the average film thickness (643 nm) is much larger than the other two domains.

Solute precipitated honeycomb structures were formed owing to solvent evaporation. The air/water interface in the present strategy for film fabrication is essential to generate

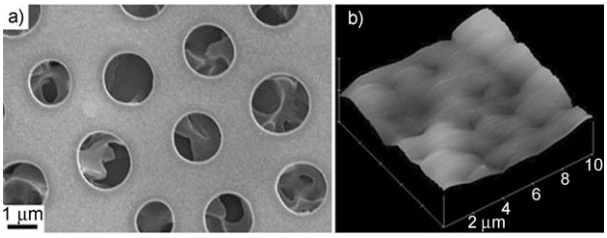

Figure 5. a) SEM and b) AFM images of the alveoli-like porous film domain. The concentration of gold nanoparticle dispersion for film fabrication is 0.8 $g L^{-1}$.

the honeycomb structures with different morphologies. In contrast, no porous structures were formed when casting on solid substrates, for example, such as using glass slides under the same conditions. Thus, the template effect of the stabilized water droplets plays an important role in the formation of ordered macroporous structures. Although the breath figure method can be used to fabricate porous films based on polymers or nanoparticles, there may not be a single, generally applicable mechanism for the formation of self-assembled array of condensed water droplets.

Korgel and co-workers have investigated the formation mechanism of macroporous thin films using perfluorothiol-stabilized gold nanoparticles cast from Freon.[14] They found that the gold nanoparticles do not reduce the interfacial tension between the Freon and water but instead reduce the Freon/water contact angle, suggesting that the nanoparticles stabilize the water droplets through the Pickering emulsion effect. Although dodecanethiol-capped gold nanoparticles have increased surface hydrophobicity, they have been shown to be effective in stabilizing condensed water droplets to form porous structures.[15,19]

Another important influence on structure formation is the solution concentration of gold nanoparticles. The change in effective nanoparticle concentration during the evaporation process can further account for the varied domain formation in the prepared thin films. In general, samples with a lower nanoparticle concentration result in a faster solvent evaporation rate. A longer water condensation and evaporation time in the middle region of the film gives rise to the hexagonal network domains with a larger pore diameter than is the domain at the edge of the film. The smallest pore size is obtained in the central area of the film, formed at the last stage of evaporation. This is possibly due to the solution reaching its saturation point rapidly, thus precipitating of the gold nanoparticles. The rapid precipitation may be faster than the condensation and self-assembly process of the water droplets on the solvent surface. At each stage of the evaporation process, the water droplets reach a self-limiting size corresponding to the feature size of the domain.

Based on the discussion above, the morphological changes in the evaporation process can be easily understood. Figure 6 illustrates the structure formation mechanism for each domain. When the radius of the water droplets is smaller than the film height (Figure 6a), a perforated mono-

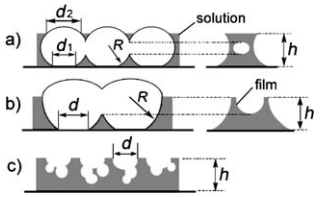

Figure 6. Illustrations for the formation mechanism of the structures of different domains: a) Perforated monolayer film domain, b) hexagonal network domain, c) and the alveoli-like porous film domain. *R*, *d*, and *h*, are the radius of the water droplet, the opening diameter of the pore, and the film height, respectively.

layer domain with pores having two openings are formed. With the formation of larger water droplets, the radius becomes larger than the film height (Figure 6b) and hexagonal network domains are obtained. The rapid precipitation of gold nanoparticles prevents the further coalescence of water droplets, so small pore sizes are obtained for the alveoli-like porous film domains (Figure 6c). It has been shown that the floating of water droplets on the surface of the solution is important for the formation of ordered pore arrays. When a solvent denser than water, such as carbon disulfide, is used, only a single layer of pores is formed.[10] In contrast, the three-dimensional pore arrays (alveoli-like porous films) were formed in the central area of the cast film (Figure 6c), although the casting solvent (chloroform in this case) is denser than water. This phenomenon may be explained by the submergence of water droplets into the organic solution under the effect of Marangoni convection. Open pore structures (no bottom layer under the pores), also due to this convection effect, were formed in the perforated monolayer domains (Figure 6a) and hexagonal network domains (Figure 6b). Contact of gold nanoparticle-stabilized water droplets must have occurred in the final stage of the film formation, as the pore arrays are interconnected (Figure 6a,b) probably owing to the surface tension effect that opens up the pore arrays when the separating wall is too thin. The three-dimensional pore arrays are also interconnected (Figure 6c) and can be understood by taking into account the evaporation of water droplets.

As the domain morphology is dependent on the effective local concentration in the evaporation process, the initial concentration of gold nanoparticles should also influence the morphologies of the fabricated thin films. Illustrate in Figures 7–9 are the results obtained from samples with varying initial concentrations of nanoparticles. Figure 7 shows the morphological changes of perforated monolayer film domains. When the concentration of gold nanoparticle is low ($0.45\,g\,L^{-1}$), a larger pore size was obtained; the structure appears to be weaker because there is an obvious shift in parts

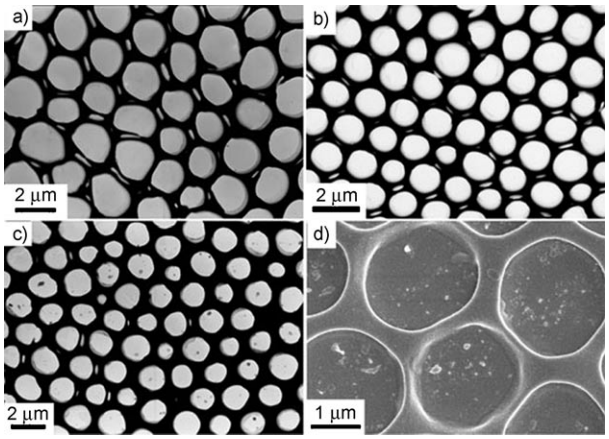

Figure 7. TEM images of the perforated monolayer film cast from samples with different concentrations of gold nanoparticles: a) $0.45\,g\,L^{-1}$, b) $0.6\,g\,L^{-1}$, c) $0.8\,g\,L^{-1}$. The SEM image d) is taken from a region in c).

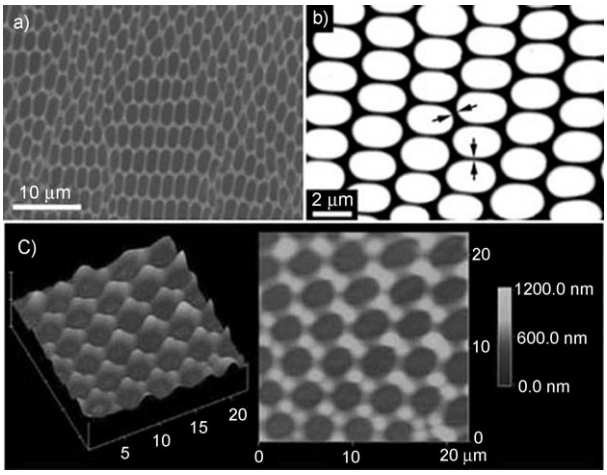

Figure 8. a) SEM, b) TEM and c) AFM images of the two-dimensional networks with deformed pore arrays. The concentration of gold nanoparticle dispersion for film fabrication is $0.45\,g\,L^{-1}$. The arrows in b) highlight the walls with two different thicknesses.

of the top and bottom layers (Figure 7a). When the concentration of gold nanoparticles is greater ($0.6\,g\,L^{-1}$), the pore array is more ordered and the pore size is more uniform; the layer shift is reduced because of the formation of stronger structure between the top and bottom layers (Figure 7b). When the concentration of gold nanoparticle is fur-

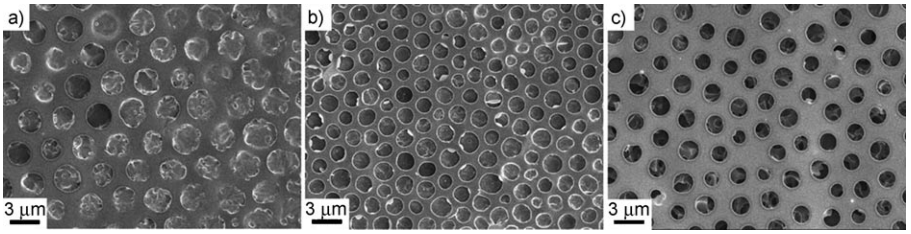

Figure 9. SEM images of the alveoli-like porous films with different casting concentrations of gold nanoparticles: a) $0.45\,g\,L^{-1}$, b) $0.6\,g\,L^{-1}$, c) $0.8\,g\,L^{-1}$.

ther increased ($0.8\,g\,L^{-1}$), hierarchical structures similar to previously reported pore-island architectures[3] were obtained (Figure 7c) and further illustrated by the SEM measurement (Figure 7d). The appearance of nanoparticle islands in the pores can be explained by the aggregation of the nanoparticles on the top of water droplets to lower the surface tension.[3] When both the water and solvent evaporate completely, the aggregates of the nanoparticles deposit into the pores and islands are formed.

The morphological changes of hexagonal network domains with varying initial concentrations of nanoparticles are more complicated. In all prepared films, both uniform hexagonal and deformed (distorted, stretched, and compressed) polygons were observed in the hexagonal domain (Figure 8a). The mobility of the film on the water surface could be an important cause of the deformation of the honeycomb film because motion of the film is inevitable owing to the asymmetric dewetting process.[20] Of more interest, some films exhibit elliptic pore arrays, some of which have a high aspect ratio. From the TEM image of such arrays (Figure 8b) it can be seen that the wall thickness of the elliptic pores in the long axis (0.35 μm) becomes larger than that of the short axis (0.25 μm) (arrows, Figure 8b). The deformation of the network can also be confirmed by the AFM image of the elliptic networks that the two adjacent knots have nearly coalesced into one knot and the pore arrays have become rhombohedrally arranged (Figure 8c). Although the morphology of these deformed structures is less uniform, self-assembly on the water surface may represent a new procedure to generate deformed structures rather than using mechanical deformation methods.[21]

Compared with the two domains discussed above, the morphological change of the alveoli-like porous structures in the centre area of the film is less significant with change in initial nanoparticle concentration (Figure 9). The average diameter of the pores slightly decreases and the pores become less ordered as a function of increased initial nanoparticle concentration. This is possibly due to the faster precipitation of the gold nanoparticles at the higher concentration, which inhibits the growth and self-assembly of the water droplets. Although both the morphological changes in film domains and the films resulting from different initial concentrations show a concentration dependent behavior, there does not appear to be a general rule concerning the relationship between the structure morphology and the nanoparticle concentration. Possibly there is some balance between the nanoparticle concentration and water droplets condensation rate induced by solvent evaporation. Indeed, one can anticipate that the formation of ordered macroporous breath figure structures is the result of the fine balance among many factors including solution concentration, humidity, and temperature.

To further examine the effectiveness of this strategy to generate porous structures at the air/water interface, DODMAC stabilized gold nanoparticles with a larger average core diameter (12.5 nm) were used as nanoparticle building blocks (Figure 10a). Using the same procedure described above resulted only in honeycomb films with two-dimensional pore arrays (Figure 10b), similar to the perforated monolayer film domains. From both the enlarged TEM (Figure 10c) and HRTEM (Figure 10d) images, one can easily discern that the wall of the film is composed of tightly packed gold nanoparticles. Although no distinct domains were observed in this fabricated film, it illustrates an additional example of using the evaporation method to fabricate macroporous structures of gold nanoparticles at the air/water interface.

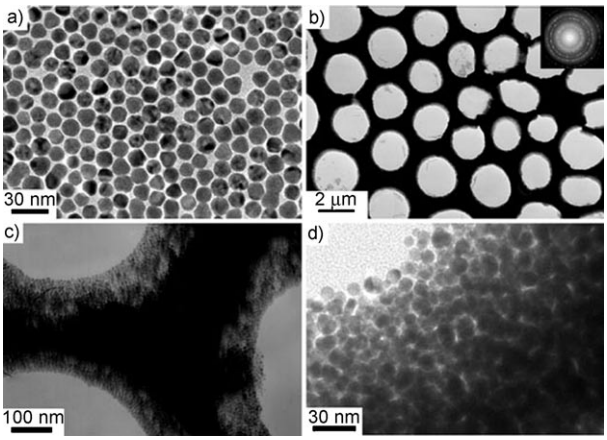

Figure 10. a) HRTEM image of DODMAC stabilized 12.5 nm gold nanoparticles. b, c) TEM and d) HRTEM images of the films formed by solvent evaporation method. The inset in b) is the electron diffraction pattern of the honeycomb films.

Finally, it should be noted that although weakly bound ligand stabilized gold nanoparticles are generally unstable and form aggregates over several weeks in dispersion, the porous films cast from DODMAC stabilized gold nanoparticles are stable over several months. DODMAC stabilized gold nanoparticles exhibit strong surface plasmon resonance absorption, while the absorption band of dodecanethiol-capped gold nanoparticles is dampened greatly due to their small size and the strong metal-ligand interactions (see the Supporting Information). The strong surface plasmon resonance together with the ligand exchange properties[22] of the weakly capped gold nanoparticles should promote the application of these honeycomb structures in surface-enhanced Raman spectroscopy, currently under investigation in this laboratory.

Conclusions

Concentration dependent ordered honeycomb structures were fabricated at the air/water interface using a solvent evaporation method. Domains of two-dimensional (perforated monolayer films and hexagonal networks) and three-dimensional pore arrays (alveoli-like porous films) were obtained in single films owing to the change of the effective nanoparticle concentration during the evaporation process. The initial nanoparticle concentration of the dispersion also

influences the morphologies of each domain. The prepared gold nanoparticle-based macroporous thin films are easily transferred onto different substrates for various applications. For instance, two-dimensional honeycomb networks may be used as soft lithography templates to create patterned materials. Formation of such porous structures at the air/water interface is not confined to gold nanoparticles and the method has been successfully extended to other nanocrystalline starting materials. In addition to the simplicity of fabrication, the proposed procedure may be easily combined with other techniques to generate structures with specific properties.

Experimental Section

Chemicals: Tetraoctylammonium bromide (TOAB) and DODMAC were purchased from Fluka. Hydrogen tetrachloroaurate trihydrate ($HAuCl_4 \cdot 3H_2O$), dodecanethiol and other chemicals were obtained from Guoyao (Shanghai, China). All chemicals were used as received without further purification.

Nanoparticle synthesis: Dodecanethiol-capped gold nanoparticles were synthesized at room temperature using an established two-phase method[23] without any size-selective process (Figure 2a). Specifically, an aqueous solution of $HAuCl_4 \cdot 3H_2O$ (0.2 mmol in 10 mL) was mixed with a solution of TOAB in toluene (0.65 mmol in 20 mL). The two-phase mixture was stirred vigorously for 30 min and the organic phase was collected. Dodecanethiol (100 μL) was added to the organic phase, and a freshly prepared aqueous solution of sodium borohydride (2.2 mmol in 25 mL H_2O) was slowly added with vigorous stirring. The organic phase changed from orange to dark brown within a few minutes. After being stirred for 12 h, the organic phase was separated, evaporated to 5 mL in a rotary evaporator and mixed with ethanol (100 mL) to remove excess thiol. The mixture was centrifuged to collect the dark brown precipitate, which was washed with ethanol five times and dried in a vacuum desiccator. DODMAC-stabilized gold nanoparticles were prepared in the same method except that DODMAC was used as both the phase transfer reagent and the capping ligand. The as-prepared gold nanoparticles capped by either dodecanethiol or DODMAC were easily redispersed in chloroform for characterization or film formation.

Honeycomb film formation: Several drops of DODMAC solution in chloroform were spread on the water surface (glass culture dish, 9 cm diameter) at room temperature till the chloroform solution can not spread but forms a lens-shaped liquid film. The gold nanoparticle dispersions in chloroform (approximately 3 μL) were then deposited onto the surfactant monolayer with a microsyringe. After several minutes, a thin opaque film formed on water surface. The thin film was transferred onto silicon wafer for AFM measurements or onto a copper grid for TEM and SEM measurements.

Characterization: TEM images were obtained by using a JEOL JEM-100CX II transmission electron microscope at an acceleration voltage of 100 kV. HRTEM images were obtained by using a JEOL JEM-2010 high-resolution transmission electron microscope at an acceleration voltage of 200 kV. SEM images were obtained by using a JEOL JSM6700F field-emission scanning electron microscope at 3.0 kV. AFM measurements were made by using a Digital Instruments NanoScope III, operating in tapping mode. Absorption spectra were acquired by using a Hitachi U4100 spectrophotometer.

Acknowledgements

The authors thank the NSFC (Grant No. 20625307) and National Basic Research Program of China (973 Program, 2009CB930103) for financial support. We also thank Dr. J. David Van Horn (Visiting Professor at Shandong University) for editorial assistance.

[1] M. P. Pileni, *Acc. Chem. Res.* **2007**, *40*, 685–693; S. A. Claridge, A. W. Castleman, Jr., S. N. Khanna, C. B. Murray, A. Sen, P. S. Weiss, *ACS Nano* **2009**, *3*, 244–255.
[2] C. J. Kiely, J. Fink, M. Brust, D. Bethell, D. J. Schiffrin, *Nature* **1998**, *396*, 444–446; X. M. Lin, H. M. Jaeger, C. M. Sorensen, K. J. Klabunde, *J. Phys. Chem. B* **2001**, *105*, 3353–3357; Y. Yang, S. Liu, K. Kimura, *Angew. Chem.* **2006**, *118*, 5790–5793; *Angew. Chem. Int. Ed.* **2006**, *45*, 5662–5665.
[3] X. Xu, X. Wang, A. Nisar, X. Liang, J. Zhuang, S. Hu, Y. Zhuang, *Adv. Mater.* **2008**, *20*, 3702–3708.
[4] A. E. Saunders, P. S. Shah, M. B. Sigman, Jr., T. Hanrath, H. S. Hwang, K. T. Lim, K. P. Johnston, B. A. Korgel, *Nano Lett.* **2004**, *4*, 1943–1948.
[5] P. M. Tessier, O. D. Velev, A. T. Kalambur, A. M. Lenhoff, J. F. Rabolt, E. W. Kaler, *Adv. Mater.* **2001**, *13*, 396–400.
[6] P. N. Bartlett, J. J. Baumberg, P. R. Birkin, M. A. Ghanem, M. C. Netti, *Chem. Mater.* **2002**, *14*, 2199–2208.
[7] A. Imhof, D. J. Pine, *Nature* **1997**, *389*, 948–951.
[8] S. A. Davis, S. L. Burkett, N. H. Mendelson, S. Mann, *Nature* **1997**, *385*, 420–423.
[9] B. De Boer, U. Stalmach, H. Nijland, G. Hadziioannou, *Adv. Mater.* **2000**, *12*, 1581–1583; P. H. Tung, S. W. Kuo, K. U. Jeong, S. Z. D. Cheng, C. F. Huang, F. C. Chang, *Macromol. Rapid Commun.* **2007**, *28*, 271–275.
[10] M. Srinivasarao, D. Collings, A. Philips, S. Patel, *Science* **2001**, *292*, 79–83.
[11] L. V. Govor, I. A. Bashmakov, R. Kiebooms, V. Dyakonov, J. Parisi, *Adv. Mater.* **2001**, *13*, 588–591.
[12] T. Nishikawa, R. Ookura, J. Nishida, K. Arai, J. Hayashi, N. Kurono, T. Sawadaishi, M. Hara, M. Shimomura, *Langmuir* **2002**, *18*, 5734–5740.
[13] T. Yonezawa, S. Onoue, N. Kimizuka, *Adv. Mater.* **2001**, *13*, 140–142.
[14] P. S. Shah, M. B. Sigman, Jr., C. A. Stowell, K. T. Lim, K. P. Johnston, B. A. Korgel, *Adv. Mater.* **2003**, *15*, 971–974.
[15] J. Li, J. Peng, W. Huang, Y. Wu, J. Fu, Y. Cong, L. Xue, Y. Han, *Langmuir* **2005**, *21*, 2017–2021.
[16] Y. Sakatani, C. Boissière, D. Grosso, L. Nicole, G. Soler-Illia, C. Sanchez, *Chem. Mater.* **2008**, *20*, 1049–1056.
[17] D. Fan, X. Jia, P. Tang, J. Hao, T. Liu, *Angew. Chem.* **2007**, *119*, 3406–3409; *Angew. Chem. Int. Ed.* **2007**, *46*, 3342–3345; P. Tang, J. Hao, *J. Colloid Interface Sci.* **2009**, *333*, 1–5.
[18] U. H. F. Bunz, *Adv. Mater.* **2006**, *18*, 973–989.
[19] F. Q. Sun, W. P. Cai, Y. Li, B. Q. Cao, Y. Lei, L. D. Zhang, *Adv. Funct. Mater.* **2004**, *14*, 283–288.
[20] C. Stowell, B. A. Korgel, *Nano Lett.* **2001**, *1*, 595–600.
[21] T. Nishikawa, M. Nonomura, K. Arai, J. Hayashi, T. Sawadaishi, Y. Nishiura, M. Hara, M. Shimomura, *Langmuir* **2003**, *19*, 6193–6201.
[22] K. G. Thomas, J. Zajicek, P. V. Kamat, *Langmuir* **2002**, *18*, 3722–3727.
[23] M. Brust, M. Walker, D. Bethell, D. J. Schiffrin, R. Whyman, *J. Chem. Soc. Chem. Commun.* **1994**, 801–802.

Received: July 29, 2009
Published online: November 13, 2009

